JMEPEG (2007) 16:710–719
DOI: 10.1007/s11665-007-9112-5

1059-9495/$19.00

Characterization of the Micro-Welding Process for Repair of Nickel Base Superalloys

J. Durocher and N.L. Richards

(Submitted November 2, 2006)

Micro-welding is a low-heat input process whereby a metal or cermet, is deposited by the generation of a low-power arc between a consumable electrode and a substrate. The low-heat input of this process offers unique advantages over more common welding processes such as gas tungsten arc, plasma arc, laser, and electron beam welding. At present, the repair of turbine blades and vanes commonly involves gas tungsten arc welding and these components are susceptible to heat affected zone cracking during the weld repair process; vacuum brazing is also used but mainly on low-stress components such as stators. In this study, the low-heat input characteristic of micro-welding has been utilized to simulate repair of Inconel (Trade Mark of Special Metals) 625, Inconel 718, and Inconel 722 filler alloys to a cast Inconel 738 substrate. The effect of micro-welding process parameters on the deposition rate, coating quality, and substrate has been investigated.

Keywords aerospace, joining, metallography, superalloys, welding

1. Introduction

In today's competitive airline market, maintenance of gas turbines is an important economic consideration for operators. Based on a pre-determined schedule, turbines are sent to repair centers for inspection, repair, and overhaul. Life limiting factors contributing to the degradation and eventual failure of gas turbine blades and vanes are: alternating stresses, impurities in the fuel, operating temperature, water ingestion, and temperature cycling. The resulting failure modes of components are rupture, creep, high, and low cycle (and thermal) fatigue, oxidation, erosion, corrosion, wear, and foreign object damage. The criticality of turbine blades also imposes heavy restrictions on the extent of repairs that can be made. In general, repairs tend to have reduced properties as compared to the base material and are limited to the upper 10-20% portion of blades where they experience the least amount of loading (Ref 1). Today's welding processes fail to produce a repaired blade where the original properties have been fully restored. Therefore, where unacceptable damage is found outside the permitted repair area, blades must be replaced. This restriction brings great potential to the development of innovative repair techniques, processes and use of materials to increase the fraction of blades that can be repaired.

Inconel 738 is a common nickel-based superalloy found in gas turbine blades and vanes. Being precipitation hardened by the γ' phase $Ni_3(Al, Ti)$ and MC type carbides, the alloy suffers from micro-cracking in the weld heat affected zone as a result of precipitation and grain boundary liquation during the weld cycle (Ref 2). This problems also affects other γ' alloys where the aluminum + titanium content is greater than about 3 wt.% (Ref 3). To minimize cracking in blade alloys, a softer solid solution strengthened alloy such as Inconel 625 is commonly used as weld filler. The resulting repair is inferior to the parent material for wear, corrosion resistance, hardness, tensile strength, fatigue, and creep resistance (Ref 1).

Current repair processes include gas tungsten arc welding (GTAW), plasma transferred arc welding (PTAW), micro-plasma transferred arc welding, laser beam welding (LBW), diffusion brazing, wide gap diffusion brazing, and transient liquid phase bonding (Ref 4). Of these processes, manual GTAW is by far the most common due to its relative low cost, simplicity, and versatility. The disadvantages of using GTAW are that the process is relatively slow, and that solid solution strengthened alloy fillers are required when welding high strength γ' precipitation hardenable alloys. The use of high strength fillers leads to severe heat affected zone micro-cracking (Ref 3). Brazing processes are not permitted on highly stressed components such as blades. Diffusion brazing is permitted for small crack repairs, limited to non-critical stationary components. The process relies heavily on cleaning and removal of oxides for proper wetting and flow of the braze alloy. Wide gap brazing is a process used to rebuild missing sections of airfoils, crack repair, and restoration of eroded wall thickness.

In light of the shortcomings of current processes, potential improvements in mechanical properties of repaired high strength nickel-based γ' turbine Superalloys, may be achieved by the development of cost-effective, low-heat input filler deposition processes. One such process is micro-welding, where a consumable electrode is held in contact and deposited onto a conductive substrate using low-pulse power levels. The resulting deposit is metallurgically bonded and re-alloyed with the substrate. The repair of a gas turbine component is considered economical if the cost of the repair does not exceed

J. Durocher, Bristol Aerospace Ltd., 660 Berry St., Winnipeg, Canada, R3C 2S4; and **N.L. Richards,** Department of Mechanical & Manufacturing Engineering, University of Manitoba, Winnipeg, Canada, R2N 5V6. Contact e-mail: nrichar@cc.umanitoba.ca.

approximately 40-60% (Ref 1) of the component's value. Therefore, the potential for a significant cost savings exists and may be achieved by low-heat input material deposition processing such as micro-welding.

The present research program, therefore, was undertaken to evaluate the effect of micro-welding process parameters on the microstructural characteristics of several filler alloys and to model these effects. Thus by understanding the process one can optimize repair of cast Inconel 738 substrates.

2. Experimental Procedures

The micro-welding electrode alloys were selected based on their current use in commonly repaired components and low concentration of gamma prime formers, namely aluminum and titanium. Table 1 shows the chemical compositions of materials used in this study. As-received cast Inconel 738 bars 6 mm thick by 25 mm wide by 175 mm long were abrasive blasted with 180 grit aluminum oxide to remove the surface scale. Using a rounded graphite electrode with a radius of 16 mm, spherical 'hemispheres,' 0.6 mm deep by 9 mm in diameter were electrical-discharge machined in the bars with a Charmilles Technologies Roboform die sinker machine. The electrical-discharge machined surfaces were subsequently removed by careful mechanical grinding with a carbide ball tool. The bars were sectioned to make individual specimens that were identified and weighed to the nearest 0.0001 g using a Mettler Toledo AG204 balance.

A CANOX C-SW300 AD/DC gas tungsten arc welding power supply was used for welding baseline weld specimens. The welding process parameters were:

- Electrode: 2% thoriated tungsten
- Filler: Inconel 625 wire
- Cover gas: argon
- Polarity: electrode negative
- Current pulse/wave: none, DC mode
- Voltage: 10 ± 1 V
- Current: 20 ± 2 A

Micro-welding equipment consists of a resistance-capacitance circuit where the electrode is in contact with the substrate. To prevent fusion of the electrode to the substrate, it is rotated or vibrated during the welding process. The micro-welding equipment used in this study was a Model PS98 MKII power supply with a manually operated AH98-MKIDD torch. Manual process parameters that were controlled in this study were:

- Cover gas: argon
- Pulse duration: 25-50 μs
- Electrode rotational speed: 1100-1200 rpm
- Torch traverse speed: 6-12 mm/s
- Orientation: 30-45° from coated surface
- Contact force: approximately 1.0 N

To date, a parametric design of experiments that quantifies the main effects and interactions between the principal micro-welding process variables has never been published in the scientific literature. The three key pulse-arc variables under study are: voltage, current, and capacitance. The pulse frequency depends on the selected parameters for voltage, current, and capacitance and is a floating variable in industrial applications. Therefore, for the purpose of this study, the arc frequency was also allowed to be a floating variable. The range of process parameters was as follows: 100-200 V, 3-5 A, and 20-50 μF. A 2-level, 3-factor with three center points design of experiments was devised for voltage, current, and capacitance. Center points are included in designs of experiments in order to determine if curvature exists in the data and repeating the center

Table 1 Chemical composition of materials (wt.%)

	IN738 (Notes 1 and 2)	IN625 (Note 3)	IN718 (Note 3)	IN722 (Note 3)
C	0.17	0.1 max	0.08 max	0.08
Co	8.5	1.0 max	1.0 max	0.0
Cr	16.0	21.5	19.0	15.5
Mo	1.7	9.0	3.0	0.0
W	2.6	0.0	0.0	0.0
Ta	1.7	...	...	0.0
Nb	0.9	3.65 (w/Ta)	5.0 (w/Ta)	0.0
Al	3.4	0.4 max	0.5	0.7
Ti	3.4	0.4 max	0.9	2.4
Al + Ti	6.8	0.8 max	1.4	3.1
B	0.01	0.0	0.006 max	0.0
Zr	0.05	0.0	0.0	0.0
Fe	0.5 max	5.0 max	Balance	7.0
Mn	0.2 max	0.5 max	0.35 max	1.0 max
Si	0.3 max	0.5 max	0.35 max	0.07 max
S	0.015 max	0.015 max	0.015 max	0.01 max
Ni	Balance	Balance	52.5 (w/Co)	Balance
Cu	0.0	0.0	0.3	0.5 max
P	0.0	0.015 max	0.015	0.0
Pb	0.0	0.0	0.0	0.0

Notes:
As-received composition
Composition of substrate and electrode material
Nominal compositions of electrode material

point measurement three times is standard practice. The responses investigated in this study were:

1. Deposition rate
2. Void content (volume fraction)
3. Crack density (total length/unit area)
4. Coating hardness (on Inconel 738 only)

Minitab[1] statistical analysis software was used to analyze the design of experiments for each response. An initial review of *p*-values provides information on the effect of terms in the DOE. The *p*-value is a calculated term ranging from 0 to 1, which describes the probability that two populations have the same mean value. Low *p*-values correspond to a high probability that the population means are different and that a particular term has a significant effect on the response. It is common practice to use a threshold *p*-value of 0.05 for the results but this can be overly restrictive in some cases. Since the goal of this study is to establish a general understanding of the micro-welding process, a threshold *p*-value of 0.1 was generally used in order to expand the process modeling results.

The micro-welding machine was setup for each combination of voltage, current, and capacitance in accordance with the design of experiments listed in Table 2. The Inconel 738 specimens were micro-weld coated in the as-received condition. For each electrode material, the hemispheres were filled with for a maximum period of 60 min, or until a mound of approximately 0.5 mm protruded above the surrounding surface in instances of high deposition rates. Initial sectioning of uncoated specimens was carried out using a Buehler abrasive wheel cutter and processed using standard metallographic procedures. Coated specimens were sectioned using a wire feed spark machine. Figure 1 shows a diagram indicating the location of sections taken from micro-welded coated specimens. To reveal the microstructure of the cast Inconel 738 base material and the micro-weld interface, Kalling's no. 2 reagent was swabbed on the polished surface for 3-5 s followed by cold tap water and distilled water rinsing. This provided a clear view of the interface but exaggerated the relative size of voids and cracks by rounding off their edges. Therefore, quantitative measurements using a Zeiss microscope with Clemex image analysis software were conducted on specimens in the as-polished and unetched condition.

Using the Clemex software, measurement routines were written to measure the area fraction of voids and total crack length. In the field of view, the gray scale level in images was converted into distinct bitmap planes and assigned a color. The software then provided measurements for the features of interest differentiated by colors. Area fraction void content measurements were taken at a magnification of 100×. This limited the maximum number of fields that could be measured on each specimen to six or seven, depending of the coating thickness. For each specimen, the measured area fractions of voids were added and the average was calculated.

The crack length measurements were taken at 200× magnification. The higher magnification permitted the detection of fine cracks in the coating. Up to ten random fields were taken on each specimen. The routine for these measurements was written such that long narrow cracks and voids were measured and the large, round voids considered to be porosity were excluded. Using the Clemex software, the total crack length for each field was measured and the average crack density for each specimen was calculated in terms of total crack length per unit area.

[1]Trade Mark of Minitab Inc.

Table 2 Design of experiments

Specimen no.	Capacitance, μF	Voltage, V	Current, A
1	20	100	3
2	50	100	3
3	20	200	3
4	50	200	3
5	20	100	5
6	50	100	5
7	20	200	5
8	50	200	5
9	30	150	4
10	30	150	4
11	30	150	4

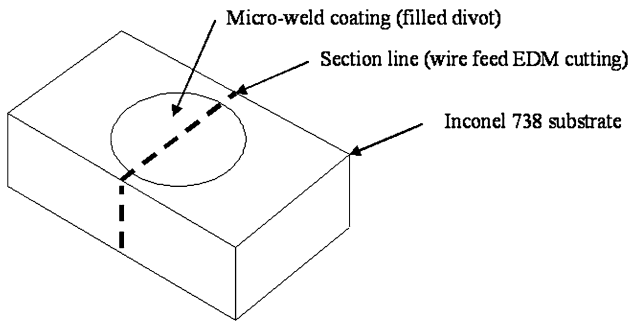

Fig. 1 Sketch showing sectioning of micro-welded coated specimens

A JEOL JSM5900LV scanning electron microscope equipped with Oxford energy dispersive spectroscopy was used for high magnification metallographic examinations. The secondary electron imaging mode was used for all examinations. Specimens were viewed with an accelerating voltage ranging from 20 to 25 kV while elemental line scans and maps were taken at 20 kV.

A Leitz Knoop hardness tester with a load of 2.942 N (300 gf) was used for all hardness measurements. Prior to use, the hardness tester was verified for accuracy with N.I.S.T traceable reference blocks within the testing hardness range. For each hardness determination, the average of three acceptable indentations was taken.

3. Results

3.1 Microstructure

3.1.1 Baseline Gas Tungsten Arc Welds. Similarly to the results obtained by Thakur et al. (Ref 2) and Banerjee et al. (Ref 3) for gas tungsten arc welded in 738, the baseline gas tungsten arc welded Inconel 738 (IN625 filler), in the as-cast form suffered from severe heat affected zone cracking. Microfissures propagated along grain boundaries into the base material while the weld metal remained crack free. Figure 2 shows a scanning electron microscope image of weld cracks in the heat affected zone. It is worth noting that liquid penetrant inspection, a common method of inspecting weld repairs would not detect the intergranular cracking beneath the filler alloy as it

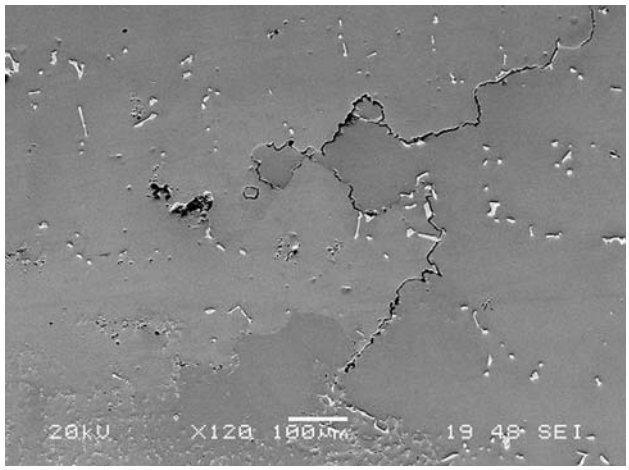

Fig. 2 Cracks in the heat affected zone of as-cast Inconel 738 gas tungsten arc welded with Inconel 625 filler. Filler is visible at lower left edge of image

can only detect surface cracks. X-ray inspection would also fail to detect the cracks because of their predominant perpendicular orientation relative to the weld repair material's surface. For detection by x-ray inspection, cracks must traverse longitudinally in the material.

3.1.2 Metallography of Micro-Welds. When viewed with optical and scanning electron microscopy, the micro-welded coating microstructures were generally featureless. In the unetched condition, individual droplets were not visible in the majority of cases. A light swab etch of the polished surface with Kalling's no. 2 reagent revealed some individual droplet deposits. When examined in the etched condition, a preferred orientation became apparent in the coatings. Fine columnar grains in the order of 3-5 µm in width were observed to be aligned perpendicular to the base material's surface. The predominant grain orientation is parallel to the axis of heat flow during the cooling phase of the micro-weld process and supports the findings of Korobeinik (Ref 5). In the coating microstructure, the individual grains appear to have been formed by several layers of deposits. Therefore, during the plasma transport mode, the deposited material would likely assume the crystallographic orientation of the base layer upon which solidification takes place. Figure 3 shows a scanning electron microscope images of the grain structure in the Inconel 625 micro-welded deposits.

As the process parameters were varied, the coatings showed varied amounts of porosity and cracking. Increasing the voltage and current increased the amount of porosity and cracks in the deposits. However, the cast Inconel 738 base material remained free of cracks and did not exhibit a heat affected zone for all parameters and alloy deposits examined in this study.

The deposit to base material interface generally exhibited good fusion and showed evidence of metallurgical bonding. Due to the high similarity in alloying constituents between the electrode alloys and the Inconel 738 substrate, EDS line scans could not accurately resolve re-alloying at the interface where metallurgical bonding and mixing occurred. As shown in Fig. 4, the Inconel 738 deposit structure has interspersed microporosity with excellent fusion to the base material. Figure 5 shows the typical Inconel 738 micro-welded microstructure using the highest power settings selected in this design of experiments. When compared to Fig. 4, a drastic difference exists in the amount of porosity and cracking in the coatings.

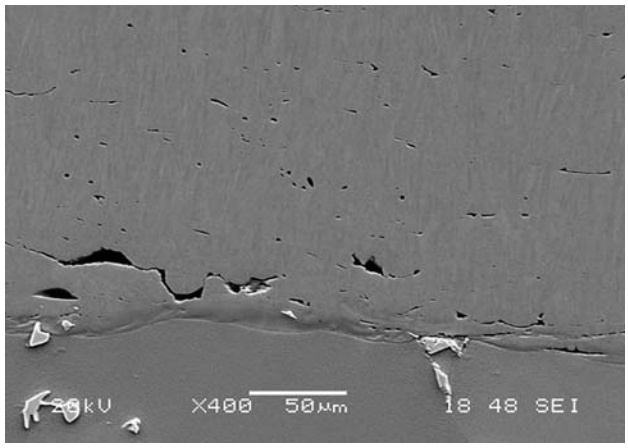

Fig. 3 SEM image of Inconel 625 micro-welded deposit showing the fine and oriented grain structure (4 A, 150 V, and 30 µF), swab etched with Kalling's no. 2 reagent

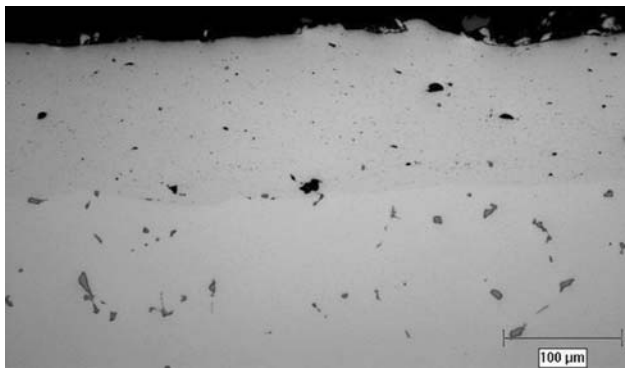

Fig. 4 Inconel 738 micro-welded deposit microstructure exhibiting a plasma deposition mechanism (3 A, 100 V, and 20 µF), unetched condition

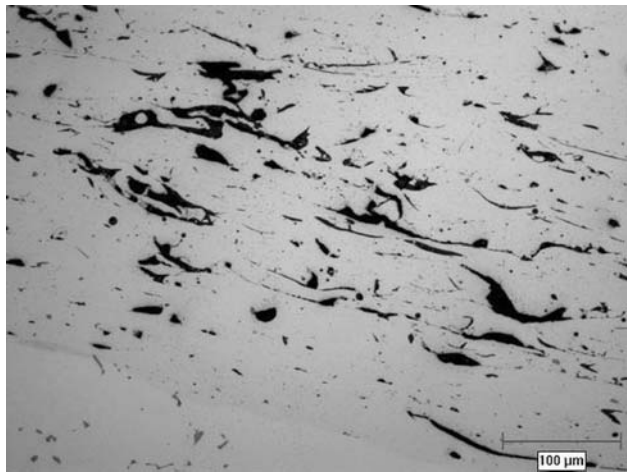

Fig. 5 Inconel 738 micro-weld deposit microstructure displaying plasma, droplet, and contact transfer mechanisms (5 A, 200 V, and 50 µF), unetched condition

As the pulse arc power is increased, a gradual shift occurs from what was predominantly complete plasma transport mechanism to a combination of plasma, droplet, and contact transport

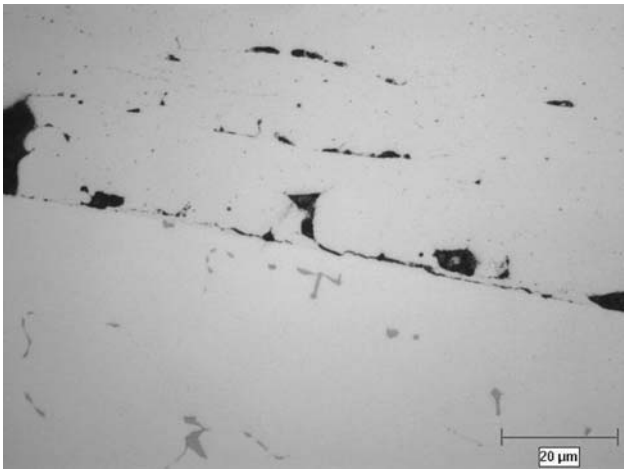

Fig. 6 Interface lack of fusion in Inconel 738 micro-welded deposit (4 A, 150 V, and 35 µF), unetched condition

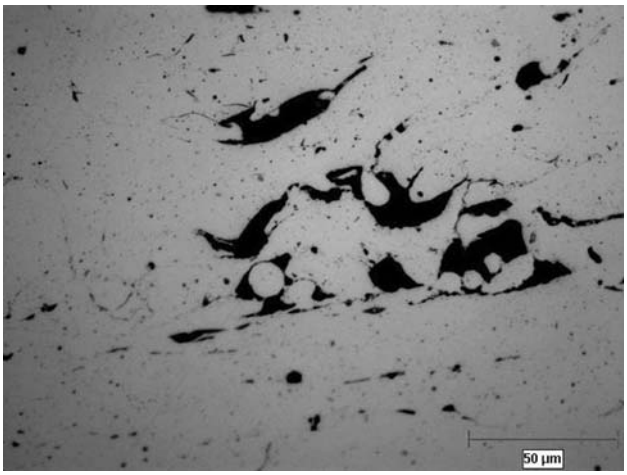

Fig 7 Cracks, porosity, and droplets in Inconel 738 micro-welded deposit (20 µF, 200 V, and 5 A), unetched condition

mechanisms. Separation between the coating and substrate was observed in one instance and is shown in Fig. 6. As current, voltage, and capacitance were increased from their base values of 3 A, 100 V, and 20 µF, the amount of porosity and cracking were observed to increase for all alloys. In Fig. 7, droplets in the coating are clearly visible and confirm the presence of this transport mechanism.

4. Statistical Analysis

Initially, the results for deposition rates, void content, and crack density were analyzed to determine which terms had a significant effect on the response. Using a threshold p-value of 0.1, significant terms were identified. Similarly, the p-values for main effects, two-way interactions, three-way interactions, and curvature were evaluated for their effect on each response. As a reference, the percentage of contribution to variation by the main effects, two-way interactions, three-way interactions, and curvature was also calculated, Table 3.

The terms considered were capacitance, voltage, current, capacitance*voltage, capacitance*current, voltage*current, and capacitance*voltage*current. In the analysis, terms were not considered to have a significant effect on the response if they had a p-value greater than 0.1. A p-value of 0.1 or less for the main effects, two-way interactions and three-way interactions was considered to indicate a significant effect on the response. A p-value less than 0.1 for the curvature was considered to have a significant contribution to variation and would therefore not provide an accurate process model.

4.1 Deposition Rate

Experimental results are shown in Appendix 1 for filler alloy 625. The analysis showed that the main effects accounted for 82.3% of the observed variation on deposition rate, Table 3. The two-way interactions and three-way interactions had no significant contributions to the variation but the curvature accounted for 4.7%. Of the main effects, only the current had a significant effect on deposition rate with a p-value of 0.068.

The general model for deposition rate is:

$$\begin{aligned}\text{Deposition rate (g/h)} &= -0.217 + 0.00279 * \text{CAPACITANCE} \\ &\quad + 0.000969 * \text{VOLTAGE} + 0.0891 * \text{CURRENT} \\ &\quad - 2.42\text{E} - 5 * \text{CAPACITANCE} * \text{VOLTAGE} \\ &\quad - 0.000545 * \text{CAPACITANCE} * \text{CURRENT} \\ &\quad - 0.000270 * \text{VOLTAGE} * \text{CURRENT} \\ &\quad + 0.00000443 * \text{CAPACITANCE} \\ &\quad * \text{VOLTAGE} * \text{CURRENT}\end{aligned}$$

with a reduced model for significant terms with p-values less than 0.1:

$$\text{Deposition rate (g/h)} = -0.0945 + 0.0528 * \text{CURRENT}$$

For filler alloy 718, Appendix 2, and Table 3, the main effects accounted for 84.0% of the observed variation in deposition rate, but both two-way interactions and three-way interactions, combined with curvature, resulted in no model being possible. The capacitance, voltage, and current terms had significant effects with p-values below 0.10. With a p-value of 0.015, the curvature in the results accounted for 5.6% of the variation.

With the use of filler alloy 722, Appendix 3 and Table 3, the main effects accounted for 83.4% of the observed variation in results while the two-way interactions and three-way interactions accounted for 15.3 and 0.01%, respectively. The voltage, current and voltage*current terms had significant effects on the deposition rate of this deposit. With a p-value of 0.270, the curvature only accounted for 0.7% of the variation in the results. The general process model for deposition rate is:

$$\begin{aligned}\text{Deposition rate (g/h)} &= 0.147 + 0.00526 * \text{CAPACITANCE} \\ &\quad - 0.00177 * \text{VOLTAGE} - 0.120 * \text{CURRENT} \\ &\quad - 4.42\text{E} - 5 * \text{CAPACITANCE} * \text{VOLTAGE} \\ &\quad + 0.000237 * \text{CAPACITANCE} * \text{CURRENT} \\ &\quad + 0.00144 * \text{VOLTAGE} * \text{CURRRENT} \\ &\quad + 0.00000333 * \text{CAPACITANCE} \\ &\quad * \text{VOLTAGE} * \text{CURRENT}\end{aligned}$$

with a reduced model for significant terms with p-values less than 0.1:

Table 3 Summary of statistical relationships

Relationship	Filler	Main effect accounted, %	Two-way interactions	Three-way interactions	Curvature, %	Comment
Deposition rate	625	82.3	1.6	0.3	4.7	Reduced model structure: main effects
	718	84.0	6.2	4.1	5.6	No possible model, strong curvature with p-value of 0.015
	722	83.4	15.3	0.01	0.7	Reduced model structure: main effects and two-way interactions
	738	87.5	8.3	1.3	1.3	Reduced model structure: main effects
Void content	625	33.0	14.3	4.8	63.6	No possible model, strong curvature with p-value of 0.023
	718	43.1	23.4	21.6	5.6	No possible model, main effects p-values >0.1
	722	53.3	24.2	12.3	9.6	No possible model, strong curvature with p-value of 0.031
	738	62.6	3.0	0.1	25.8	Reduced model structure: main effects
Crack density	625	40.5	6.3	1.6	48.9	No possible model, strong curvature with p-value of 0.025
	718	17.8	19.1	4.7	57.7	No possible model, strong curvature with p-value of 0.005, main effects p-values were >0.1
	722	16.8	32.1	42.8	1.2	No possible model, main effects p-values were >0.1
	738	64.5	20.4	11.8	0.007	Reduced model structure: main effects

$$\begin{aligned}\text{Deposition rate (g/h)} &= 0.321 - 0.00331 * \text{VOLTAGE} - 0.111 * \text{CURRENT} \\ &\quad + 0.00156 * \text{VOLTAGE} * \text{CURRENT}\end{aligned}$$

Using filler alloy 738, Appendix 4 and Table 3, the main effects accounted for 87.5% of the observed variation in deposition rate. The capacitance, voltage, and current terms had significant effects with p-values below 0.10. With a p-value of 0.322, the curvature in the results accounted for 1.3% of the variation.

The general model for deposition rate is:

$$\begin{aligned}\text{Deposition rate (g/h)} &= -0.517 + 0.0114 * \text{CAPACITANCE} \\ &\quad + 0.00238 * \text{VOLTAGE} + 0.120 * \text{CURRENT} \\ &\quad - 0.000105 * \text{CAPACITANCE} * \text{VOLTAGE} \\ &\quad - 0.00326 * \text{CAPACITANCE} * \text{CURRENT} \\ &\quad - 0.000256 * \text{VOLTAGE} * \text{CURRRENT} \\ &\quad + 0.0000369 * \text{CAPACITANCE} \\ &\quad * \text{VOLTAGE} * \text{CURRENT}\end{aligned}$$

with a reduced model for significant terms with p-values less than 0.1:

$$\begin{aligned}\text{Deposition rate (g/h)} &= -0.907 + 0.00481 * \text{CAPACITANCE} \\ &\quad + 0.00286 * \text{VOLTAGE} + 0.161 * \text{CURRENT}\end{aligned}$$

4.2 Void Content

With filler alloys 625, 718, and 722, Appendices 1-3 and Table 3, the combination of main effects, two-way interactions and three-way interactions, gave low-model accuracies, while curvature showed significant effects. Therefore, an accurate process model for the effect of process parameters on void content could not be generated.

For filler alloy 738, Appendix 4 and Table 3, the main effects for void content accounted for 62.6% of the observed variation while the two-way interactions, three way interactions, and curvature accounted for 3.0, 0.01, and 25.8%, respectively. With a p-value of 0.061, current was the only term with a value below 0.10. The general process model for void content is:

$$\begin{aligned}\text{Void content (vol.\%)} &= -8.23 + 0.0317 * \text{CAPACITANCE} \\ &\quad + 0.0378 * \text{VOLTAGE} + 2.7 * \text{CURRENT} \\ &\quad - 0.000367 * \text{CAPACITANCE} * \text{VOLTAGE} \\ &\quad - 0.00500 * \text{CAPACITANCE} * \text{CURRENT} \\ &\quad - 0.00883 * \text{VOLTAGE} * \text{CURRRENT} \\ &\quad + 0.0000667 * \text{CAPACITANCE} \\ &\quad * \text{VOLTAGE} * \text{CURRENT}\end{aligned}$$

with a reduced model for significant terms with p-values less than 0.1:

$$\text{Void content (vol.\%)} = -2.85 + 1.55 * \text{CURRENT}$$

4.3 Crack Density

With the use of filler alloys 625, 718, and 722, Appendices 1-3 and Table 3, the main effects were low and curvature again showed too high values resulting in no models possible.

With 738 filler deposits, Appendix 4 and Table 3, the main effects for crack density accounted for 64.5% of the variation while the two-way interactions, three-way interaction, and curvature accounted for 20.4, 11.8, and 0.007%, respectively. The voltage and current terms had, with p-values of 0.076 and 0.039, respectively, had significant effects on the crack density. The general process model for crack density is:

$$\begin{aligned}\text{Crack density } (\mu\text{m}/\mu\text{m}^2) &= -0.0244 + 0.000660 \\ &\quad * \text{CAPACITANCE} + 0.000201 * \text{VOLTAGE} \\ &\quad + 0.00735 * \text{CURRENT} - 6.48\text{E} - 6 * \text{CAPACITANCE} \\ &\quad * \text{VOLTAGE} - 0.000200 * \text{CAPACITANCE} * \text{CURRENT} \\ &\quad - 5.32\text{E} - 5 * \text{VOLTAGE} * \text{CURRRENT} + 1.97\text{E6} \\ &\quad - * \text{CAPACITANCE} * \text{VOLTAGE} * \text{CURRENT}\end{aligned}$$

with a reduced model for significant terms with p-values less than 0.1:

$$\text{Crack density } (\mu m/\mu m^2) = -0.0108 + 0.0000378 * \text{VOLTAGE} + 0.00271 * \text{CURRENT}$$

4.4 Inconel 738 Coating Micro-Hardness

As the pulse power increased, Appendix 4, the resulting deposit hardness decreased while the substrate hardness remained effectively unchanged; note that no cracks were found in the base material microstructure. The moderately higher hardness values measured with low-pulse energies were likely caused by the formation of a near-amorphous structure as a result of higher cooling rates achieved with less heat input.

Using the statistical analysis software, a design of experiment analysis was carried out on the hardness results for the Inconel 738 micro-welded deposit. The main effects accounted for 56.4% of the measured variation on hardness, while two-way interactions and three-way interactions accounted for 12.9 and 30.3%, respectively. The curvature accounted for only 0.3% of the observed variation. Therefore, since the main effects, two-way interactions and three-way interaction all had *p*-values less than 0.1, a model can be written as follows:

$$\begin{aligned}\text{HK} = {} & 230 + 8.58 * \text{CAPACITANCE} + 1.80 * \text{VOLTAGE} \\ & + 45.5 * \text{CURRENT} - 0.0620 * \text{CAPACITANCE} \\ & * \text{VOLTAGE} - 1.95 * \text{CAPACITANCE} * \text{CURRENT} \\ & - 0.408 * \text{VOLTAGE} * \text{CURRENT} + 0.0137 \\ & * \text{CAPACITANCE} * \text{VOLTAGE} * \text{CURRENT}\end{aligned}$$

An increase in capacitance, voltage or current caused a decrease in coating hardness. Changing the current from the low value to the high value had the largest effect on reducing the coating hardness. Figure 8 shows the micro-hardness profiles for the lowest and highest pulse energy settings.

5. Discussion of Results

As summarized in Tables 4-6, the analysis for the factorial design of experiments showed in general that: voltage and current have the most significant effect on deposition rate, void content, and crack density of micro-welded deposits. In nearly all cases, changing the capacitance did not have a significant effect on the response.

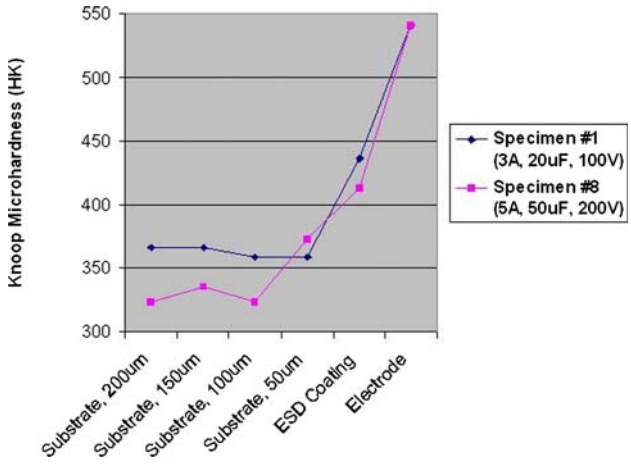

Fig. 8 Knoop hardness measurements for the lowest (above) and highest (below) pulse arc power settings

In several instances, the curvature in the result accounted for a significant portion of the variation as confirmed with *p*-values greater than 0.1. From the process models generated in this study, the following observations can be made:

- For highest deposition rates, the voltage and current must be set to their maximum values (200 V, 5 A).
- For lowest void content, and crack density, the voltage and current must be set to their minimum values (100 V, 3 A).
- Capacitance has little effect on the deposition rate, void content, and crack density of micro-weld deposits.
- For harder coatings, the capacitance, voltage, and current must be set to their minimum values (30 μF, 100 V, and 3 A).

During the micro-welding process, the electrode is in vibration and traverses the substrate. This causes a range of microtopographies that can be classified into three groups: plasma, droplet, and contact transport mechanism (Ref 5). The plasma transport topography is generally featureless while droplets can be readily seen in the microstructure when the droplet transport mechanism operates. The zone of contact transport comprises of droplets destroyed during the electrode contact and is seen as bridging within the coating. The zone of plasma transport has the best service properties of the three types. It has maximum hardness and highest protection against wear and corrosion. It is also relatively high in chemical homogeneity. The zone of contact transport has the worst properties of the three possible transport mechanisms.

Since the conditions for high deposition rate and low porosity and cracking cannot be satisfied simultaneously, the user must have a predetermined maximum amount of tolerable defects in the coating. Then, the process parameters that yield the highest deposition rate capable of maintaining the porosity and cracking within acceptable levels can be used. In the present research, the process parameters were shown to have a significant effect on the microstructure of micro-welded deposits. With low voltage and current values, the deposits were relatively featureless and free of defects. This indicates that the plasma transport mechanism described in Korobeinik (Ref 5) is predominant under these conditions. The absence of a distinct interface between the deposit and base material is confirmation that micro-weld deposits are metallurgically bonded to the base material. At high voltage and high current values, the deposits showed increased amounts of porosity, cracks, and lack of fusion to the base material. In all but one model, capacitance was shown to have no significant effect on deposition rate, void content or crack density in the deposits.

Process parameters were also shown to have a significant effect on the deposit's hardness for Inconel 738. An increase in capacitance, voltage or current decreased the deposit's hardness. Low values for capacitance, voltage, and current reduced the pulse power and heat input during the welding process. Therefore, with a reduced heat input, the solidification rate of the material being deposited increases. As described by Johnson (Ref 6), the high solidification rates associated with low-pulse power settings can result in amorphous or near-amorphous deposits. In the present study, a fine columnar grain structure could be resolved for all deposits when viewed in the etched condition. Therefore, it is probable that only near-amorphous structures were obtained.

Table 4 Process model coefficients for deposition rate

Model for deposition rate, g/h

$Y = A + B * \text{CAPACITANCE} + C * \text{VOLTAGE} + D * \text{CURRENT}$
$- E * \text{CAPACITANCE} * \text{VOLTAGE} - F * \text{CAPACITANCE} * \text{CURRENT}$
$- G * \text{VOLTAGE} * \text{CURRRENT} + H * \text{CAPACITANCE} * \text{VOLTAGE} * \text{CURRENT}$

Alloy	*A*	*B*	*C*	*D*	*E*	*F*	*G*	*H*
IN625	−0.0945	...	...	0.0528	...	...	...	...
IN722	0.321	...	−0.00331	−0.111	...	...	0.00156	...
IN738	−0.907	0.00481	0.00286	0.161	...	...	...	...

Process models could not be generated when *p*-values greater than 0.10 were obtained

Table 5 Process model coefficients for void content

Model for crack density, μm/μm²

$Y = A + B * \text{CAPACITANCE} + C * \text{VOLTAGE} + D * \text{CURRENT}$
$- E * \text{CAPACITANCE} * \text{VOLTAGE} - F * \text{CAPACITANCE} * \text{CURRENT}$
$- G * \text{VOLTAGE} * \text{CURRRENT} + H * \text{CAPACITANCE} * \text{VOLTAGE} * \text{CURRENT}$

Alloy	*A*	*B*	*C*	*D*	*E*	*F*	*G*	*H*
IN738	−2.85	...	...	1.55	...	...	...	...

Process models could not be generated when *p*-values greater than 0.10 were obtained

Table 6 Process model for crack density

Model for crack density, μm/μm²

$Y = A + B * \text{CAPACITANCE} + C * \text{VOLTAGE} + D * \text{CURRENT}$
$- E * \text{CAPACITANCE} * \text{VOLTAGE} - F * \text{CAPACITANCE} * \text{CURRENT}$
$- G * \text{VOLTAGE} * \text{CURRRENT} + H * \text{CAPACITANCE} * \text{VOLTAGE} * \text{CURRENT}$

Alloy	*A*	*B*	*C*	*D*	*E*	*F*	*G*	*H*
In738	−0.0108	...	3.78E−5	0.00271	...	...	...	...

Process models could not be generated when *p*-values greater than 0.10 were obtained

An important observation in this study has been the absence of a heat affected zone and associated cracking in the cast Inconel 738 base material. As shown by Thakur (Ref 2) and Banerjee (Ref 3), GTAW of Inconel 738 results heat affected zone micro-fissuring caused by the high heat input during the welding process. However, the present micro-weld deposition rates are low compared to GTAW and may not be a cost effective alternative in certain applications. The micro-welding process is a potentially viable alternative to GTAW processing for build-up of surfaces on cast Inconel 738, where micro-fissuring in the parent material will results in inferior operating conditions in the turbine. In instances where voids, cracks or lack-of-fusion must be kept to a minimum, the process voltage and current must be set to their low values of 100 V and 3 A. Low values for capacitance, voltage, and current are to be used to produce harder and wear resistant coatings.

6. Conclusions

Micro-welding with alloys Inconel 625, Inconel 718, and Inconel 722 was used to evaluate the effect of process parameters on deposition rate, void content, and crack density. The effect of process parameter on the micro-weld deposit hardness was also evaluated for Inconel 738 deposited onto itself.

Conclusions are as follows:

- Voltage and current have significant effects on the deposition rate, void content, and crack density of micro-welded deposits. The greatest deposition rates were obtained with high values for voltage and current (200 V, 5 A). The void content and crack density can be reduced by using low values for voltage and current (100 V, 3 A). The capacitance did not have a significant effect on the void content and crack density in the deposits.
- Capacitance, voltage, and current were found to have a significant effect on the deposit's hardness. Increasing each of the parameters caused a decrease in the deposit's hardness. High cooling rates during the micro-welding process are responsible for the increased coating hardness.
- Process models were generated for the effects of capacitance, voltage, and current on deposition rate, void content, crack density and deposit hardness. With a threshold *p*-value of 0.1, process models could not be generated for all results. High curvature in the results prohibited the generation of some process models.
- Micro-welding is a suitable process for the application of nickel-based alloys covering a nominal range of 0.8-6.8 wt.% aluminum + titanium concentration. For all

micro-weld filler alloys tested in this study, the cast Inconel 738 base material remained free of heat affected zone micro-cracks. Based on microstructural properties alone, micro-welding appears to be superior to GTAW for the repair of turbine components made from Inconel 738 and other high strength γ' precipitation strengthened alloys.

7. Appendix

Appendix 1: Inconel 625 Micro-Weld Deposit

Specimen no.	Capacitance, μF	Voltage, V	Current, A	Frequency, Hz floating variable	Deposition rate, g/h	Void content, vol.%	Crack density, μm/μm^2
1	20	100	3	160	0.0671	1.7	0.00122
2	50	100	3	720	0.0690	2.3	0.00222
3	20	200	3	370	0.0612	2.1	0.00241
4	50	200	3	450	0.0304	2.1	0.00227
5	20	100	5	610	0.1872	1.9	0.00205
6	50	100	5	1100	0.1830	2.0	0.00287
7	20	200	5	450	0.1450	2.1	0.00265
8	50	200	5	310	0.1347	2.1	0.00314
9	30	150	4	610	0.0976	1.5	0.00342
10	30	150	4	260	0.1790	1.6	0.00314
11	30	150	4	450	0.1286	1.7	0.00364

Appendix 2: Inconel 718 Micro-Weld Deposit

Specimen no.	Capacitance, μF	Voltage, V	Current, A	Frequency, Hz floating variable	Deposition rate, g/h	Void content, vol.%	Crack density, μm/μm^2
1	20	100	3	700	0.0563	6.0	0.00962
2	50	100	3	310	0.1346	2.6	0.00546
3	20	200	3	370	0.1700	2.4	0.00546
4	50	200	3	160	0.2595	2.3	0.00566
5	20	100	5	1120	0.1566	1.9	0.00658
6	50	100	5	500	0.4046	2.7	0.00696
7	20	200	5	610	0.5175	2.6	0.01287
8	50	200	5	260	0.5014	1.7	0.01057
9	30	150	4	460	0.3669	2.4	0.01408
10	30	150	4	460	0.3504	1.4	0.01419
11	30	150	4	460	0.3393	2.7	0.01305

Appendix 3: Inconel 722 Micro-Weld Deposit

Specimen no.	Capacitance, μF	Voltage, V	Current, A	Frequency, Hz floating variable	Deposition rate, g/h	Void content, vol.%	Crack density, μm/μm^2
1	20	100	3	720	0.0942	3.1	0.00494
2	50	100	3	310	0.1706	3.9	0.00532
3	20	200	3	380	0.2811	5.0	0.00938
4	50	200	3	160	0.2548	3.8	0.00786
5	20	100	5	1120	0.1658	5.1	0.00824
6	50	100	5	510	0.2764	5.7	0.00253
7	20	200	5	590	0.6540	5.9	0.00219
8	50	200	5	270	0.6819	15.3	0.00958
9	30	150	4	450	0.3264	3.4	0.00538
10	30	150	4	450	0.2648	3.3	0.00675
11	30	150	4	450	0.2735	4.4	0.00843

Appendix 4: Inconel 738 Micro-Weld Deposit

Specimen no.	Capacitance, μF	Voltage, V	Current, A	Frequency, Hz floating variable	Deposition rate, g/h	Void content, vol.%	Crack density, μm/μm^2	Knoop micro-hardness (300p)
1	20	100	3	740	0.0479	1.0	0.00189	436
2	50	100	3	320	0.1151	1.0	0.00195	455
3	20	200	3	390	0.2216	1.8	0.00494	451
4	50	200	3	160	0.3068	1.3	0.00329	407
5	20	100	5	1120	0.2529	4.7	0.00582	422
6	50	100	5	500	0.3457	4.8	0.00568	406
7	20	200	5	620	0.5231	4.0	0.00612	410
8	50	200	5	270	0.8554	4.0	0.01610	413
9	30	150	4	470	0.4462	3.8	0.00671	427
10	30	150	4	470	0.3254	6.0	0.00386	
11	30	150	4	470	0.3893	4.4	0.00639	

References

1. General Electric Power Systems, publication # GER-3957B, "Gas Turbine Repair Technology," April 2001
2. A. Thakur, N.L. Richards, and M.C. Chaturvedi, On Crack-Free Welding of Cast Inconel 738, *Int. J. Join. Mater.*, 2003, **15**(4), p 21–25
3. K. Banerjee, N.L. Richards, and M.C. Chaturvedi, Effect of Filler Alloys on HAZ Cracking in Pre-Weld Heat Treated IN-738 LC GTA Welds, *Metall. Mater. Trans.*, 2005, **36A**, p 1881–1890
4. D.S. Duvall and J.R. Doyle, Gas Turbine Conference & Products Show, Washington D.C., April 8-12, 1973, ASME Report #73-GT-44, "Repair of Turbine Blades and Vanes"
5. F. Korobeinik, S.I. Rudyuk, and S.V. Korobeini, Characteristics of the Formation of Microtopography, Microstructure and Substructure of the Surface Layer During Electro-Spark Alloying, *Elektronnaya Obrabotka Materialov*, 1989, **1**, p 16–19
6. R.N. Johnson, "Electro-Spark Deposition: Principles and Applications," Society of Vacuum Coaters 45th Annual Technical Conference, April 2002, p 87–92